AGU PUBLICATIONS

JGR

Journal of Geophysical Research: Oceans

RESEARCH ARTICLE

10.1002/2014JC010116

Companion to *Guerrero et al.* [2014], doi:10.1002/2014JC010113.

**Special Section:**
Early scientific results from the salinity measuring satellites Aquarius/SAC-D and SMOS

**Key Points:**
- Cross-shelf exchanges in the SW Atlantic are characterized by SSS anomalies
- Cross-shelf exchanges are partially controlled by local winds
- Seasonal variations of the cross-shelf exchanges are small

**Supporting Information:**
- Readme
- Movie

**Correspondence to:**
R. P. Matano,
rmatano@coas.oregonstate.edu

**Citation:**
Matano, R. P., V. Combes, A. R. Piola, R. Guerrero, E. D. Palma, P. Ted Strub, C. James, H. Fenco, Y. Chao, and M. Saraceno (2014), The salinity signature of the cross-shelf exchanges in the Southwestern Atlantic Ocean: Numerical simulations, *J. Geophys. Res. Oceans*, *119*, 7949–7968, doi:10.1002/2014JC010116.

Received 2 MAY 2014
Accepted 1 OCT 2014
Accepted article online 17 OCT 2014
Published online 25 NOV 2014



# The salinity signature of the cross-shelf exchanges in the Southwestern Atlantic Ocean: Numerical simulations

**Ricardo P. Matano[1], Vincent Combes[1], Alberto R. Piola[2], Raul Guerrero[3], Elbio D. Palma[4], P. Ted Strub[1], Corinne James[1], Harold Fenco[3], Yi Chao[5], and Martin Saraceno[6]**

[1]College of Earth, Ocean and Atmospheric Sciences, Oregon State University, Corvallis, Oregon, USA, [2]Departamento Oceanografía, Servicio de Hidrografía Naval and Departamento de Ciencias de la Atmósfera y los Océanos, Universidad de Buenos Aires, and UMI/IFAECI, CONICET, Buenos Aires, Argentina, [3]Instituto Nacional de Investigación y Desarrollo Pesquero, Mar del Plata, Argentina, [4]Departamento de Física, Universidad Nacional del Sur and Instituto Argentino de Oceanografía, Bahía Blanca, Argentina, [5]Remote Sensing Solutions, Inc., Barnstable, Massachusetts, USA, [6]Centro de Investigaciones del Mar y la Atmósfera, and Departamento de Ciencias de la Atmósfera y los Océanos, Universidad de Buenos Aires, and UMI/IFAECI, CONICET, Buenos Aires, Argentina

**Abstract** A high-resolution model is used to characterize the dominant patterns of sea surface salinity (SSS) variability generated by the freshwater discharges of the Rio de la Plata (RdlP) and the Patos/Mirim Lagoon in the southwestern Atlantic region. We identify three dominant modes of SSS variability. The first two, which have been discussed in previous studies, represent the seasonal and the interannual variations of the freshwater plumes over the continental shelf. The third mode of SSS variability, which has not been discussed hitherto, represents the salinity exchanges between the shelf and the deep ocean. A diagnostic study using floats and passive tracers identifies the pathways taken by the freshwater plumes. During the austral winter (JJA), the plumes leave the shelf region north of the BMC. During the austral summer (DJF), the plumes are entrained more directly into the BMC. A sensitivity study indicates that the high-frequency component of the wind stress forcing controls the vertical structure of the plumes while the low-frequency component of the wind stress forcing and the interannual variations of the RdlP discharge controls the horizontal structure of the plumes. Dynamical analysis reveals that the cross-shelf flow has a dominant barotropic structure and, therefore, the SSS anomalies detected by Aquarius represent net mass exchanges between the shelf and the deep ocean. The net cross-shelf volume flux is 1.21 Sv. This outflow is largely compensated by an inflow from the Patagonian shelf.

## 1. Introduction

This article discusses the offshore detrainments of the freshwater discharges from the RdlP and the Patos/Mirim Lagoon. Previous studies have established some of the most conspicuous characteristics of these plumes, most notably, their seasonal migrations along the continental shelf of South America and their relation to the alongshelf wind forcing [*Piola et al*., 2000; *Soares et al*., 2007a, 2007b; *Palma et al*., 2008]. There are, however, no previous studies on the fate of these plumes as they move away from the coast. This gap in our understanding reflects the lack of observations to characterize this phenomenon. Earlier studies identified the TS signature of the RdlP waters in the deep-ocean region [*Gordon*, 1989; *Provost et al*., 1996] but the data used in these studies lacked the spatial and temporal resolution to establish whether the observed intrusions were a robust feature of the regional circulation or just the fingerprints of random events. In a companion article, *Guerrero et al*. [2014] (G14 hereafter) uses Aquarius SSS data to characterize, for the first time, the offshore extrusions of the RdlP waters. This article extends the observational study of G14 by addressing those topics that are beyond the spatial and temporal resolution of the Aquarius data. Both studies attempt to address the same questions, namely *What are the characteristics of the offshore extrusions of RdlP waters?* and *What are the dynamical mechanisms responsible for these extrusions?*

## 2. Background

The RdlP is one of the largest rivers of the world and the second largest of the southern hemisphere (after the Congo River). It discharges ~24,000 $m^3/s$ of silt laden waters onto the continental shelf of the southwestern Atlantic region. This freshwater injection, which is strengthened by smaller contributions from the

Patos/Mirim Lagoon (~2000 $m^3/s$), creates a freshwater plume that spreads along the coastlines of Argentina, Uruguay, and Brazil and into the deep ocean (G14). The alongshelf extension of the RdlP plume varies with the seasons [*Möller et al*., 2008; *Piola et al*., 2008a, 2008b]. During the winter it extends farther downstream, reaching as far north as 28°S, while during the summer it retracts to 32°S [*Piola et al*., 2000]. The RdlP plume also spreads in the upstream direction, extending nearly 300 km south of the mouth of the estuary [*Piola et al*., 2000]. These upstream extensions are driven by the internal dynamics of the flow and by the local wind forcing [*Soares et al*., 2007b; *Palma et al*., 2008; *Matano and Palma*, 2010a, 2010b, 2013]. Here we use the term "downstream/upstream" to mean "north/south of the river outfall," indicating the direction of propagation of coastally trapped waves in the southern hemisphere [*Matano and Palma*, 2010a].

The alongshelf displacements of the RdlP plume are partly controlled by external forcing (tides and winds) and partly by internal dynamics. Tidal forcing is important in the inner portion of the estuary, where it contributes to the formation of a strong frontal system [*Guerrero et al*., 1997; *Framiñán et al*., 1999; *Simionato et al*., 2001]. Tidal amplitudes, however, decrease rapidly in the offshore direction becoming negligible over the shelf [*Palma et al*., 2004b]. Local wind forcing appears to be the main driver of the plume spreading over the shelf. The local winds are relatively weak (~0.05 Pa) but they undergo large seasonal variations [*Palma et al*., 2004a]. During the winter, southwesterly winds (downwelling favorable) trap the plume against the coast pushing it in the downstream direction. During the summer, northeasterly winds (upwelling favorable) reverse the direction of the plume spreading causing a cross-shelf expansion of the river waters. The seasonal variations of the RdlP discharge are small but the interannual variations are quite large, ranging between extremes of 11,000 and 80,000 $m^3/s$ [*Piola et al*., 2005]. This high variability is associated with El Niño/La Niña events [*Depetris et al*., 1996]. The impact of these variations on the plume characteristics remains uncertain. *Piola et al*. [2005] noted that, during some Niño years, high river discharges are correlated with the development of anomalous northeasterly winds, which cancel the plume's natural tendency to extend farther downstream.

It is a serendipitous coincidence that the RdlP, which is one of the largest rivers of the world, discharges into the region where the waters advected from the Argentinean and the Brazilian shelves converge and detrain into the deep ocean. The RdlP discharge generates a SSS signal that tags the outflow of shelf waters into the deep ocean (beyond the shelfbreak). The paucity of the data record, however, had prevented the characterization of these off-shelf fluxes until the arrival of data acquired by the Aquarius and the SMOS missions. In a companion article, G14 use these data to broadly characterize these off-shelf fluxes. In this article, we expand this analysis using the results of a high-resolution numerical simulation. We identify the dynamical mechanisms controlling the seasonal and interannual displacements of the RdlP plume over the continental shelf and the eventual detrainment of these waters into the deep ocean.

## 3. Model Description

The model used in this study is the Regional Ocean Modeling System (ROMS), which is a three-dimensional, free surface, hydrostatic, eddy-resolving primitive equation ocean model. ROMS uses orthogonal curvilinear coordinates in the horizontal and sigma, terrain following coordinates in the vertical [*Shchepetkin and McWilliams*, 2005]. We use the version ROMS_AGRIF (http://roms.mpl.ird.fr/), which offers the capability of a two-way nesting procedure with high-resolution "child" grids embedded into a coarser resolution "parent" grid. The parent grid extends 360° in the longitudinal direction and from Antarctica to 15.2°N (Figure 1). It has a spatial resolution of 1/4°, and 40 sigma levels in the vertical, with enhanced resolution at the surface. The first child grid extends from 82°W to 41°W and from 64°S to 20°S, covering the southern portion of South America with spatial resolution of 1/12° (Figure 1). The nested configuration (parent and first child) is forced by the three day averaged ERA_Interim data set from 1979 to 2012 at the surface and by the climatology Simple Ocean Data Assimilation model (SODA) at the open boundary of the parent model (15.2°N). A detailed technical description of this model configuration, as well as its performance, can be found in *Combes and Matano* [2014]. The 10 day averaged model solution of this nested configuration is used offline as the lateral boundary conditions for a second child grid from 2000 to 2012. The second child grid extends from 66°W to 44°W and from 44°S to 25°S, thus covering the southwestern Atlantic region with a horizontal resolution of 1/24° (Figure 1), which is ~3.8 km at the latitude of RdlP mouth. Unlike the two ways nested

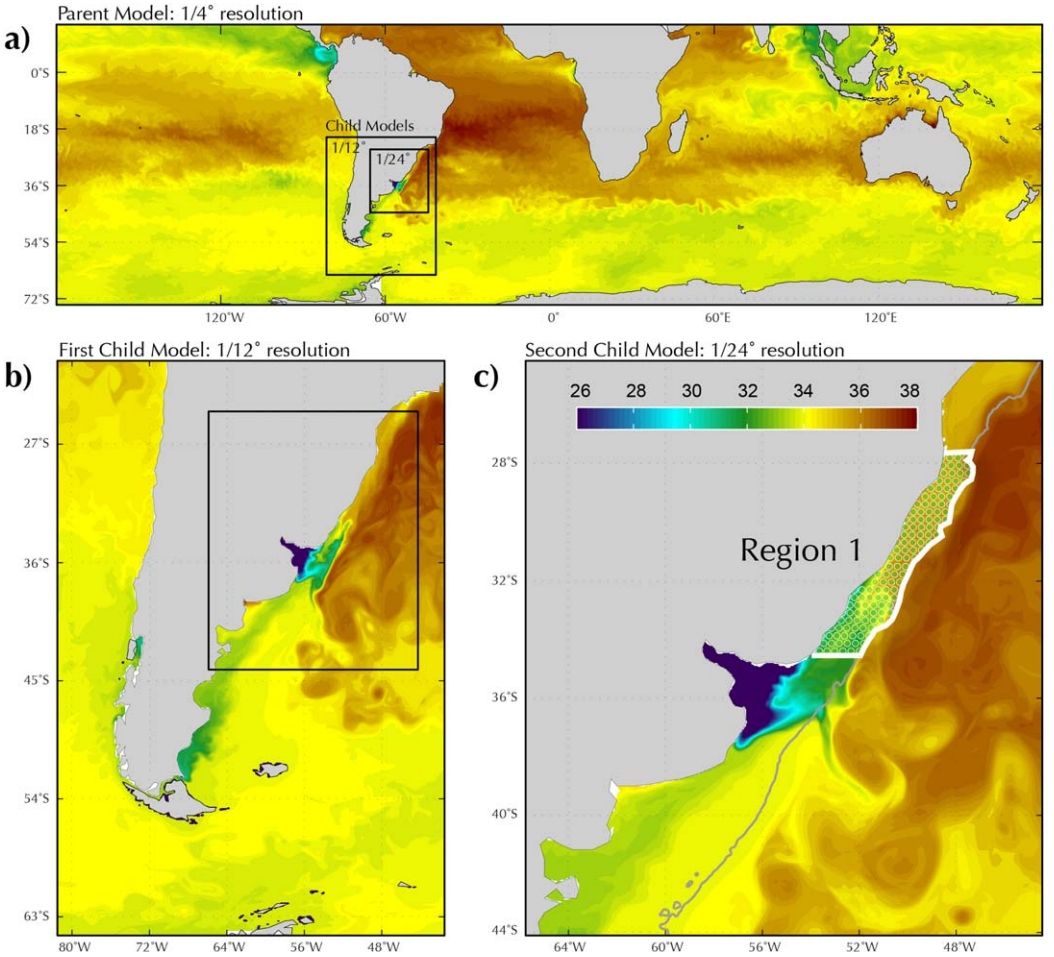


**Figure 1.** Snapshots of the sea surface salinity (SSS) in the nested model configuration used in this study. (a) The domain of the parent model, which has a horizontal resolution of 1/4°. (b) The first child model, which has a resolution of 1/12°. (b) The second child model, which has a resolution of 1/24°. The three models have the same vertical resolution (40 sigma levels). (c) The extent of Region 1, which is discussed in later sections. The gray line in Figure 1c marks the location of the 200 m isobath (the shelfbreak).

experiment of the parent and first child grids, we opted for the higher-resolution (0.25°) QuickSCAT (period 2000–2007) and ASCAT (period 2008–2012) daily wind stress as surface momentum forcing. The surface heat and freshwater fluxes are derived from the COADS data set (climatology). The model also includes a daily discharge of the RdlP, a constant discharge from the Patos Lagoon (set to 2000 $m^3/s$) and five tidal components (M2, S2, N2, K1, and O1 harmonics). The 1/24° resolution model had first spun up for the period 2007–2012, which gave the initial condition to the 2000–2012 model integration. The transport pathways and statistics of the RdlP waters are also characterized using a passive tracer advection-diffusion equation that is identical to that used for the temperature and salinity. The tracer is continuously released (set to 1) in the mouth of the RdlP and distributed from surface to bottom. Although surface forcing is averaged daily, all following analyses will use 10 day averaged fields (including wind stress).

## 4. SSS Variability and External Forcing

### 4.1. The SSS Variability of the Shelf Region

To assess the variability of the shelf region, we first compare the time series of the SSS and the wind stress forcing averaged over Region 1 (Figure 1) and the time series of RdlP discharge (Figure 2). The time series of the alongshelf winds is modulated by strong seasonal oscillations between southwesterly winds (i.e., from the southwest) during the winter and northeasterly winds (i.e., from the northeast) during the summer. There is a strong correspondence between the alongshelf winds and the SSS anomalies [*Piola et al.*, 2005;

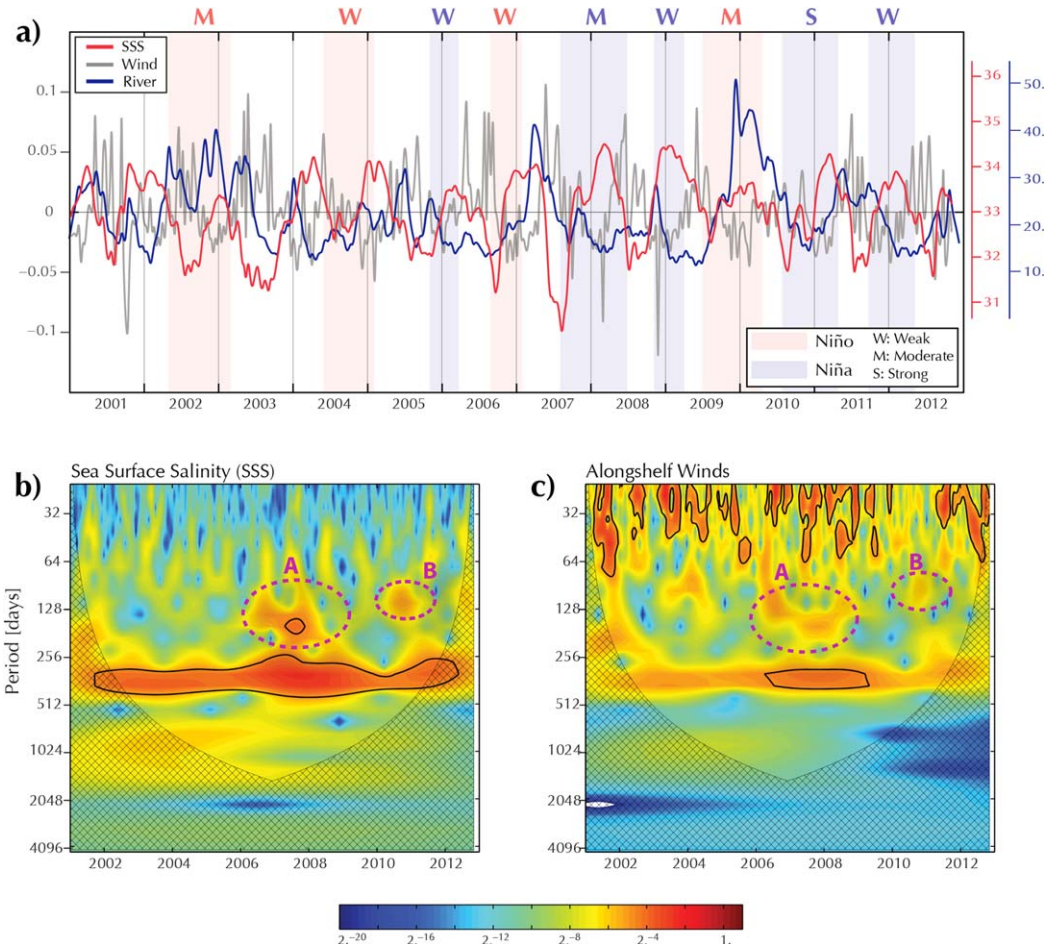


**Figure 2.** (a) Time series of the sea surface salinities (SSS) averaged over Region 1 (red line), the alongshelf component of the wind stress forcing averaged over Region 1 (gray line) and the Rio de la Plata (RdlP) discharge (blue line); (b) wavelet spectra of the time series of the SSS averaged over Region 1; (c) idem for the alongshelf wind stress forcing. The black contours show regions with a confidence level higher than 95%. Hatched regions indicate the cone of influence. The time series for the wavelet analyses have been normalized thus the color bar does not have units.

*Soares et al*., 2007b; *Palma et al*., 2008]. During the winter, southwesterly winds create geostrophic currents that advect the relatively freshwaters of the RdlP toward the north, thus generating negative SSS anomalies over the downstream region. These patterns reverse during the summer when northeasterly winds reverse the direction of the currents, which advect salty waters from the Brazilian shelf to the south, thus generating positive (saltier) SSS anomalies. The average time lag between the peaks of the winds and the peaks of the SSS anomalies is approximately 45 days, which can be interpreted as the time that it takes to change the average SSS of Region 1.

The time series of the RdlP discharge does not show any significant seasonal variations, instead it is characterized by large interannual variations (Figure 2a). A portion of this interannual variability can be associated with El Niño events, but not all. The surges of 2002 and 2009/2010, for example, followed moderate Niños but the peaks of 2005 and 2007 occurred several months after relatively weak events. The RdlP response to El Niño is highly variable, both in terms of amplitude and phase shift. This variability emerges from the distinct nature of the subbasins contributing to the river discharge. The Paraguay River forms a large and flat watershed which includes *El Pantanal*, an extensive flood territory that, when dry can hold large volumes of water for several months, and when wet discharges most volume quite fast [*Clarke*, 2005]. In contrast, the Uruguay River subbasin covers a relatively steep portion of the continent and changes in precipitation there drive rapid responses in Plata outflow. Thus, the RdlP outflow response to precipitation critically depends on precipitation distribution within the basin, and, in certain subbasins, on the recent evolution of the water balance.

A coherence spectrum (not shown) indicates that the maximum correlation between alongshelf winds and SSS occurs at the annual period ($r = 0.95$, statistically significant at a 99% confidence level), with a phase lag of approximately 45 days. To assess the spectral characteristics of the SSS and the wind stress time series we did a Morlet wavelet analysis that considers the bias rectification [*Torrence and Compo*, 1998; *Liu et al*., 2007] (Figures 2b and 2c). The spectral analysis shows that the SSS variability is concentrated in the low-frequency band and the wind stress variability is concentrated in the high-frequency band. Both time series show spectral peaks during 2006–2008 and 2010–2011 with 3–6 months periods (dotted circles A and B in Figures 2b and 2c). These peaks represent quite different hydrometeorological conditions (Figure 2a). The 2010–2011 peak corresponds to a moderate El Niño event, which began in the winter of 2009 and lasted until the end of the summer of 2010. During this period, there was a large increase of the RdlP discharge, which reached a maximum of 53,000 $m^3/s$ during December 2009 (Figure 2a). This exceptional discharge, however, did not produce a freshening of Region 1 during the summer months but a relatively small freshening during the following spring. The reduced impact of the increment of the RdlP discharge during the summer of 2010 is associated with a weakening of the southwesterly winds during the fall season. In fact, this period is largely characterized by the dominance of northeasterly winds, which would tend to arrest the downstream development of the RdlP plume. Note that the two periods of freshening during the spring of 2010 and beginning of the summer of 2010–2011 occurs in conditions of below average river discharge but southwesterly winds. The conditions observed during the 2009/2010 period are similar to those described by *Piola et al*. [2005], who reported that during the 1998 El Niño the effects of the wind and precipitation anomalies compensate each other, thus preventing a freshening of the downstream region.

The spectral peak of 2006–2008 is associated with different wind and river conditions. The peak of SSS energy at the end of 2007 was preceded by a relatively weak El Niño, which, nonetheless, led to a substantial increase of the RdlP discharge (42,000 $m^3/s$) during the summer of 2007. Although the magnitude and duration of the increase of the RdlP discharge that followed the 2006 El Niño were smaller than those observed during the 2009 event, the 2006 El Niño led to a larger freshening of Region 1, because the increment of the discharge was accompanied by a period of strong southwesterly winds, which moved the plume farther downstream. *Piola et al*. [2005] speculated that a similar combination of large river discharge and strong southwesterly winds during the fall and winter of 1992 should have produced a substantial freshening of Region 1, whether this happened is unknown. The relatively moderate El Niño of 2002 did not produce an isolated peak of the RdlP discharge, but several smaller peaks that extended through the summer of 2003 (Figure 2a). This Niño was characterized by the dominance of southwesterly winds. The combined effect of the increased river discharge and southwesterly winds generated a freshening of the shelf that extended from the fall of 2002 to the end of the spring of 2003, interrupted by higher salinities during northeasterly winds in spring-summer 2002–2003. This event is not apparent in the wavelet analysis because its dominant period is larger than those of the previous cases. Thus, the spectral peak corresponding to this event merges with the spectral peak of the seasonal cycle.

In summary, we found no definite pattern of SSS variability representing the El Niño events. The moderate Niño of 2009/2010, for example, led to an SSS increase while the equally moderate Niño of 2002/2003 led to an SSS decrease. The lack of a definite SSS response pattern to these events reflects the high variability of the alongshelf wind stress associated with them. Some Niños are associated with northeasterly winds (e.g., 2006 and 2009), others with southwesterly winds (e.g., 2002) and still others have no well-defined wind direction (e.g., 2004). Over a longer period, *Piola et al*. [2005] noted that during 1950–2001 there are relatively few episodes in which southwesterly winds and a marked freshening of the downstream region follow increases of the river discharge. During the period analyzed herein, La Niña events are characterized by below average RdlP discharges and northeasterly winds, both of which tend to increase the shelf's SSSs (in the downstream region) (Figure 2a). During the 1950–2001 period [*Piola et al*., 2005, Figure 4], however, La Niña events were characterized by a decrease of the RdlP discharge but there was no definite pattern of wind direction.

### 4.2. EOF Analysis

To further characterize the SSS variability of the southwestern Atlantic region, we computed the Empirical Orthogonal Functions (EOFs) of the time series of the SSS anomalies (Figure 3). A Monte Carlo simulation indicates that the first three EOF modes are statistically significant at the 95% level [*Preisendorfer*, 1988]. These modes account for approximately half (52%) of the total SSS variance. The first EOF, which explains

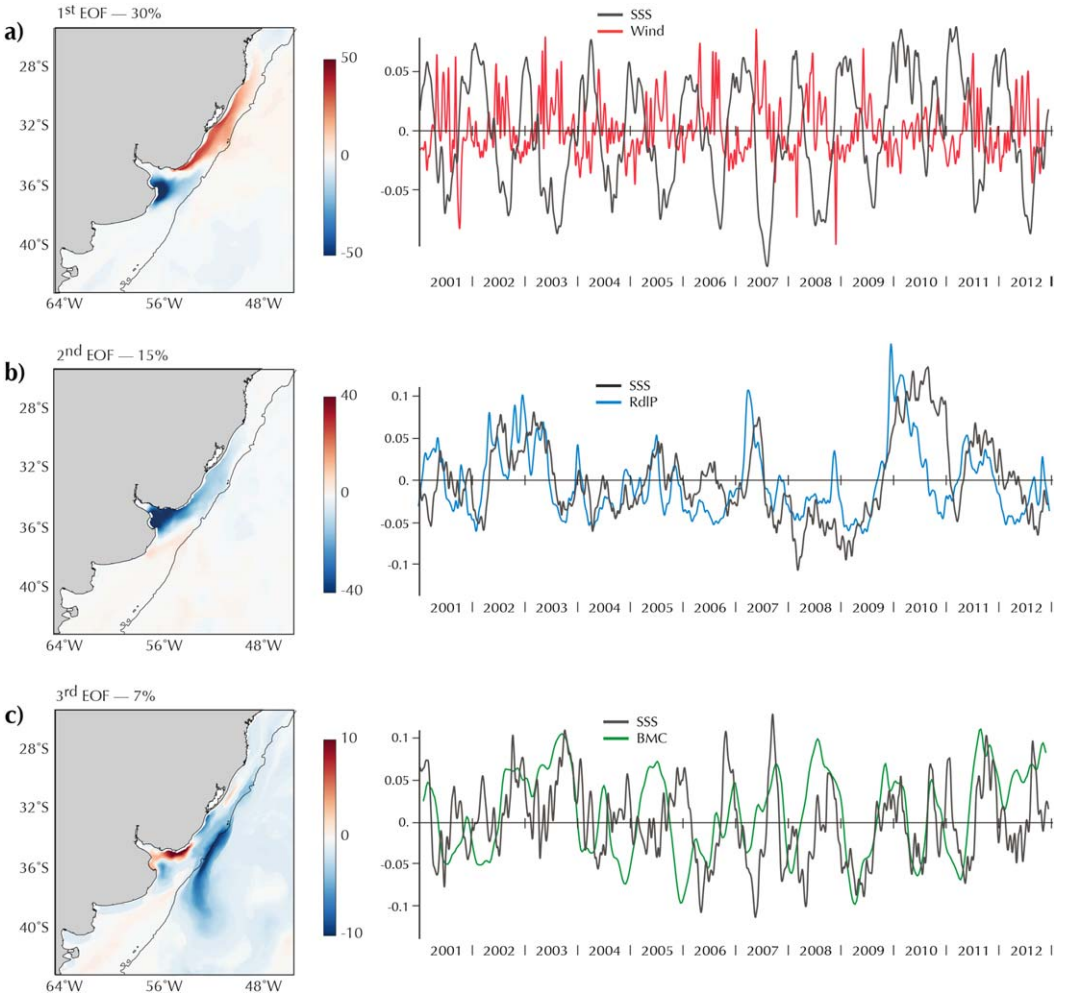


**Figure 3.** EOF modes of SSS variability (a) first mode, the red line in the time series represents the alongshelf component of the wind stress; (b) second mode, the blue line in the time series represents the LPR discharge; (c) third mode, the green line in the time series represents the latitudinal variations of the BMC. The scale for the BMC location is shown in Figure 4a.

30% of the variance, represents seasonal oscillations of the freshwater plumes along the shelf (Figure 3a). The spatial structure of this mode is characterized by a dipole structure, with lobes of opposing sign in the downstream and upstream regions. The upstream lobe, which extends from the mouth of the RdlP to 37°S, has a peak in the Samborombom Bay, which is a shallow ($h < 20$ m) indentation of the coast that is characterized by its large SSS variations [*Möller et al*., 2008, G14]. The downstream lobe extends from the mouth of the RdlP until Cape Santa Marta (~28°S). The time series of the first EOF is dominated by seasonal oscillations that are correlated ($r = 0.51$, with a maximum correlation lag of 20 days, wind lead SSS, significant at the 99% level), with the seasonal oscillations of the alongshelf winds (Figure 3a). During the summer, northeasterly winds help to move salty waters from the north Brazilian shelf toward the downstream region and fresh RdlP waters toward the upstream region creating the dipole shown in the first EOF. During the winter, winds reverse direction and move saltier waters from the Patagonian shelf into the upstream region and relatively freshwaters from the RdlP into the downstream region reversing the sign of the first EOF. The lack of strong seasonal variations of the RdlP discharge contributes to the dominance of the wind forcing on the seasonal variations of its plume (the discharge from the Patos Lagoon is kept constant in our simulation). The discrepancies between the wind and the EOF time series are mostly related to the fact that the former includes strong intraannual and interannual variations while the later does not.

The second EOF mode accounts for approximately 15% of the total SSS variance (Figure 3b). Its amplitude is characterized by an absolute maximum at the river mouth. This mode represents the impact of the RdlP discharge on the salinities of the shelf. This relationship is demonstrated by the high correlation between the

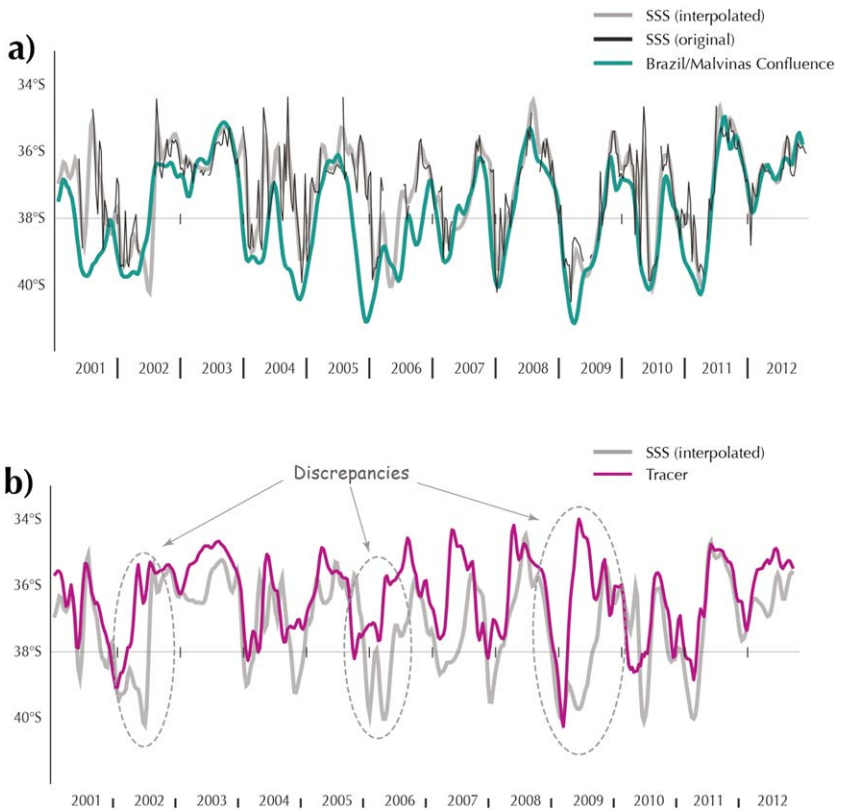


**Figure 4.** (a) Time series of the escape latitude calculated using the SSS criterion (Els). The thin, black line represents the original time series, the thick gray line the interpolated value and the green line the time series of the latitudinal variations of the BMC. (b) Time series of the escape latitude calculated using the passive tracer (ELt, purple line) and using the SSS criterion (ELs, gray line).

time series of the EOF and the RdlP discharge ($r = 0.67$, statistically significant at a 99% confidence level), both of which show similar peaks during the different phases of the El Niño/La Niña events (Figure 3b). There is an approximate 60 days lag between the two time series, which can be interpreted as the time that it takes to the SSSs over the shelf to notice the variations of the river discharge.

The third EOF mode represents the SSS anomalies associated with the exchanges between the continental shelf and the deep ocean (Figure 3c). This mode only explains 7% of the total variance, however, an ancillary EOF calculation (not shown) indicates that if the SSS data over the shelf is excluded this EOF becomes the leading mode of SSS variability, explaining 25% of the total variance. That is, the relatively small percentage of the total variability accounted by the third EOF mode only reflects the fact that SSS variations over the shelf are much larger than those over the deep ocean. The spatial structure of the third EOF is characterized by a maximum that extends along the coast of Uruguay and a minimum that spreads as a tongue that extends from the middle shelf into the deep ocean. The largest amplitudes of this tongue are observed over the shelfbreak, in the latitudinal range extending from approximately 37°S to 32°S. This tongue follows the contour of the BMC, thus suggesting a relation between the offshore detrainment of the shelf waters and the dynamics of the western boundary currents.

In the following sections, we will discuss in more detail the relation between the offshore fluxes of low-salinity waters and the dynamics of the western boundary currents. For the present purposes, we note the close correspondence between the time series of this EOF and the time series of the latitudinal location of the BMC, which was defined as the latitude where the 10° isotherm at 200 m crosses the 1000 m isobath [*Goni and Wainer*, 2001; *Combes and Matano*, 2014]. The BMC has a well-defined seasonal cycle, being displaced to the north during the winter and to the south during the summer [*Olson et al*., 1988; *Matano et al*., 1993; *Goñi and Wainer*, 2001; *Combes and Matano*, 2014]. The time series of the third EOF shows a similar seasonal cycle with fresher waters exiting the shelf during the summer months and saltier waters during the winter. The correlation between the time series of the EOF and the BMC, however, is far from perfect.

In fact, there are periods, e.g., 2001–2002 and 2004–2005, in which the time series are in opposite phase. These matters will be discussed in more detail in section 6.

In summary, we identify three dominant modes of SSS variability. The first two, which have been extensively discussed in previous works [*Piola et al*., 2000, 2008a; *Moller et al*., 2008], represent the seasonal variations of the RdlP and the Patos/Mirim freshwater plumes over the continental shelf. These modes are driven by the alongshelf component of the wind stress forcing and by interannual variations of the RdlP discharge. The third mode of SSS variability, which has not been discussed hitherto, represents the SSS anomalies associated with the exchanges between the southwestern Atlantic shelf and the deep ocean. The close correspondence between the time series of this mode and the time series of the latitudinal location of the BMC suggests that the offshore flux of the shelf waters is influenced by the dynamics of the western boundary currents.

## 5. The Salinity Signal of the Shelf/Deep-Ocean Exchanges

### 5.1. The Latitudinal Variations of the RdlP Outflows

The previous analysis suggests that the outflow of the RdlP waters into the deep ocean is controlled by the dynamics of the western boundary currents. To ascertain this relation we compare the time series of the latitude at which the RdlP waters leave the shelf, which we call ELs (*E*scape *L*atitude according to the *s*alinity criterion) with the time series of the location of the BMC. We define RdlP waters as waters with a shelfbreak SSS $< 34.0$, and the escape latitude as the middle point of the shelfbreak region with an outflow of waters with a SSS $< 34.0$ (black thin line in Figure 4a). Sometimes, we have more than one ELs (see also Movie_SSS in supporting information). In those cases, and if the different escape regions are separated by more than $0.5^\circ$, we choose as the ELs the middle point of the southernmost region. This definition produces a discontinuous time series because there are periods in which there is no outflow of waters with the specified SSS criteria. We fill the gaps in the time series using a cubic spline interpolation (thick gray line in Figure 4a).

The time series of the ELs is highly variable (Figure 4a) (see also Movie_SSS in supporting information). In general, the ELs is in the south during the summer and in the north during the winter. There are, however, exceptions to this rule. The pattern, for example, reverses during 2010, while during 2003 most of the ELs remains near $36^\circ$S during the entire year. The time variations of the escape latitude are in sync with those of the alongshelf wind forcing i.e., it is located southward during periods of strong northeasterly winds and northward during periods of strong southwesterly winds. As we shall show, however, local winds are only a complementary (albeit important) element in the removal of the RdlP waters from the shelf. The high correlation, $r = 0.76$ (99% confidence level), between the time series of the ELs and the BMC indicates that the outflow of the RdlP waters from the shelf is largely controlled by the circulation patterns established by the western boundary currents. This control is expected since the Brazil and Malvinas currents generate a barotropic pressure gradient that extends into the shelf controlling the outer shelf circulation [*Palma et al*., 2008; *Matano et al*., 2010].

We utilize a passive tracer to ascertain the location where the river waters leave the shelf. The tracer is released in the inner portion of the RdlP estuary, where it is uniformly distributed from the surface to the bottom. The spatial and temporal evolution of the tracer is controlled by an advection-diffusion equation similar to that used for the temperature and salinity fields. The latitude of escape of the tracer is defined as the shelfbreak latitude with a tracer concentration larger than 0.01. We call ELt the escape latitude according to the tracer criterion. The fact that the tracer concentration is zero everywhere allows us to follow it even when it is diluted to very low values. This calculation is more precise than the one using salinity, where mixing can make the plume's waters indistinguishable from the ambient waters as demonstrated below.

The use of a tracer as a proxy of the RdlP waters decreases the correlation with the BMC ($r = 0.70$). The correlation between ELs and ELt is $r = 0.55$ (statistically significant at the 99% confidence level). The winter months show the largest differences between the two time series (Figure 4b). Typically, during these months the ELt is located north of the ELs and the BMC (Figure 4a). This difference indicates that our definition of the ELs does not always capture the outflow of RdlP waters. During the winter months, in particular, the passive tracer indicates that the RdlP waters leave the shelf north of the BMC and the location suggested by the ELs criterion. This difference is probably due to the fact that there are shelf waters with no RdlP mixtures than are slightly fresher than 34.0.

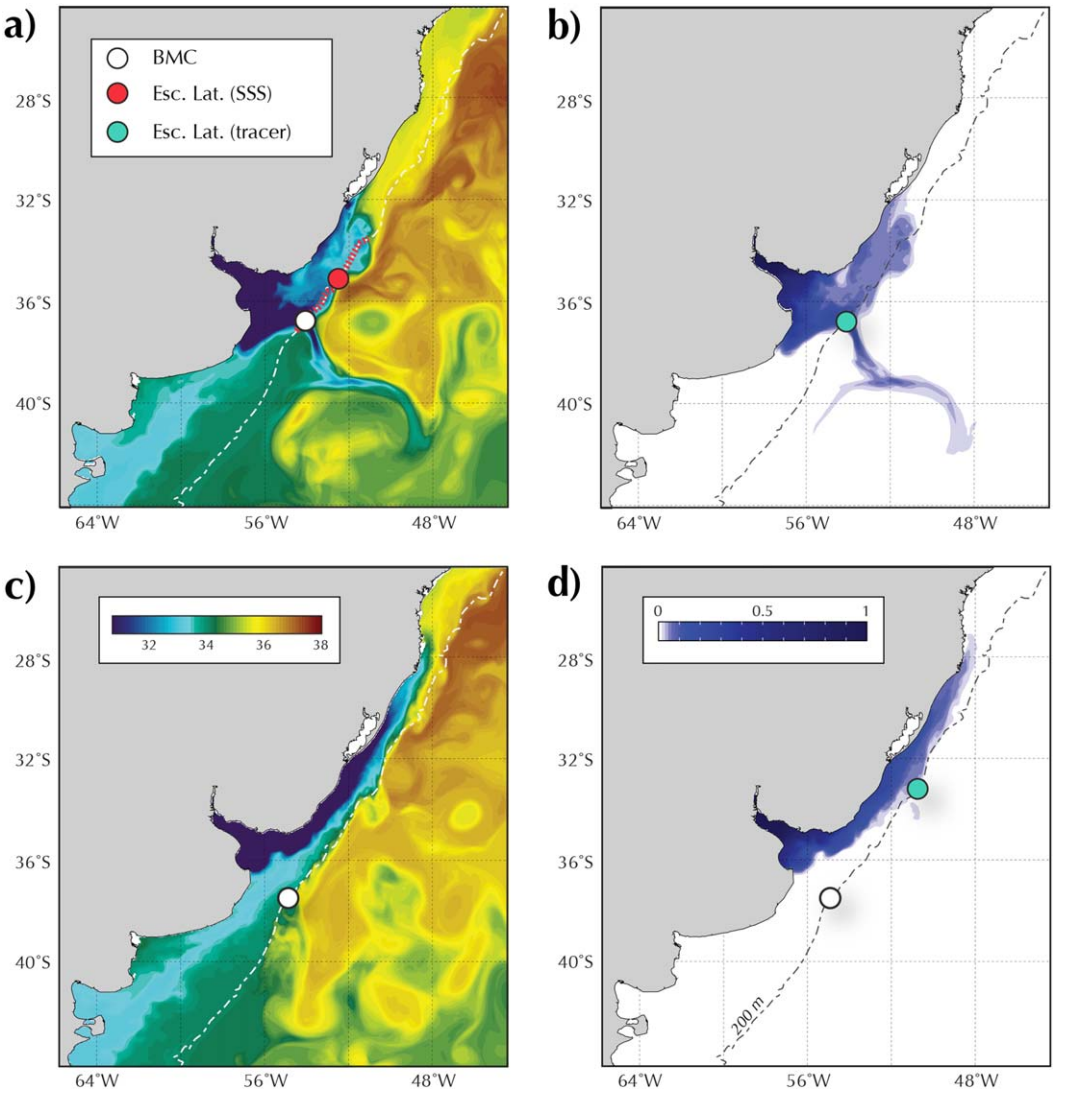


**Figure 5.** Snapshots of the (a and c) SSS and (b and d) the passive tracer. The white dots mark the location of the BMC, the red dots marks the escape latitude according to the SSS criterion and the green dot marks escape latitude according to the passive tracer. In (a and b), the location of the BMC coincides with the escape latitude according to the tracer. In (c and d), the escape latitude according to the SSS criterion cannot be determined. The red dotted line in Figure 5a shows the shelfbreak section with salinities smaller than the established criterion for RdlP waters. In situations like this, we choose the escape latitude as the middle point of this section.

Snapshots of the SSS and the tracer illustrate the causality of the differences between the ELs and the ELt estimates (Figure 5). The snapshots show the locations of the BMC (white dots), ELs (red dots) and Elt (green dots) during the summer and winter seasons. The summer snapshot corresponds to a period of northeasterly winds, which impede the alongshelf advance of the RdlP plume, thus leading to the development of a bulge of relatively freshwaters in front of the river mouth. During this event there is a long swath along the shelfbreak of waters with SSS $<$ 34.0 (dotted red line in Figure 5a). The ELs, which is defined as the midpoint of this region, is located to the north of the BMC. The ELt is located just at the BMC (Figure 5b). The difference between both estimates is relatively small. The winter months show the largest differences between ELs and ELt (Figures 5c and 5d). Downwelling favorable winds during this period trap the freshwater plume along the coast where it is advected alongshore (Figure 5c). After reaching Cape Santa Marta ($\sim$28°S) the plume is returned south by an inshore intrusion of the BC flowing along the shelfbreak. Intense mixing along this pathway increases the plume's salinity so by the time it reaches the BMC these waters have a SSS $>$ 34.0. This explains the gaps of the ELs time series during the winter months (Figure 4a). In the particular example shown here, the ELs coincide with the latitude of the BMC but it does not mark the location

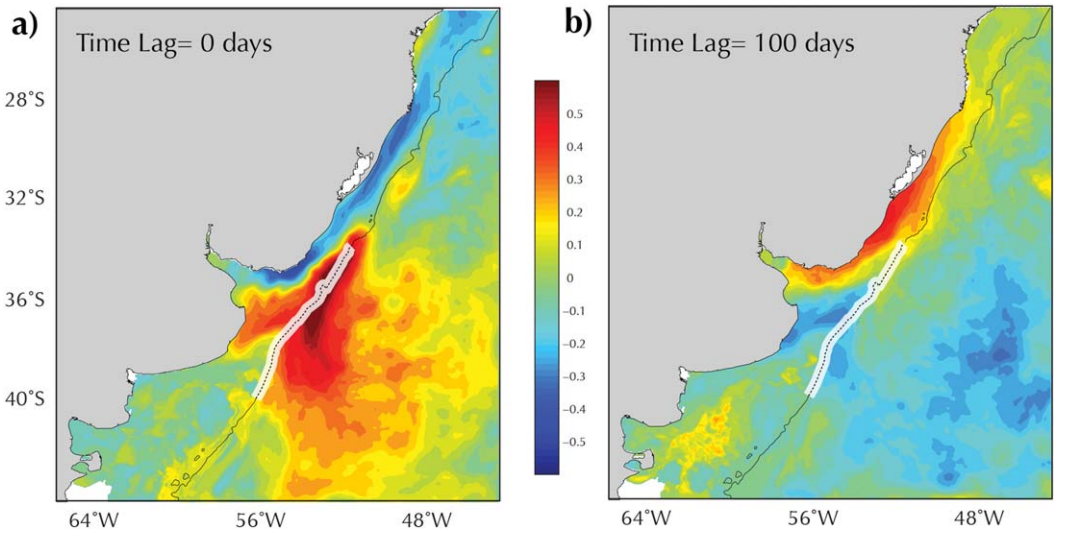


**Figure 6.** Correlations between the time averaged passive tracer concentration over the shelfbreak and the tracer concentration over all the grid points of the child model. (a) Using a time lag of 0 days; (b) using a time lag of 100 days. The thick white line with the stippled line in Figures 6a and 6b mark the shelfbreak region that we used to construct the time series of the averaged shelfbreak tracer concentration. The black contour marks the location of the shelfbreak (200 m isobath).

where the RdlP waters are detrained from the shelf. Instead, it marks the latitude of detrainment of relatively freshwaters advected from the Patagonian shelf. The RdlP waters (according to the ELt criterion) are detrained farther north, near the mouth of the Patos/Mirim Lagoon (Figure 5d). Similar detrainments through filaments have been reported from in situ observations [*Piola et al*., 2008b].

### 5.2. The Offshore Detrainment of the RdlP Waters

We use the passive tracer experiment to establish the correlation patterns that lead to the offshore detrainment of the RdlP plume from the shelf. To this end, we calculate point correlations between the time series of the tracer concentration at the shelfbreak and the time series of all the grid points of the model (Figure 6). The shelfbreak time series represents the average tracer concentration in the section that extends from 33°S to 39°S (Figure 6). Maximum correlations are observed at 0 and 100 day time lags. Note that our analysis is based on 10 day averages of the model variables; therefore a 0 day time lag represent processes with a decorrelation time scale smaller than 10 days. The correlations at zero-lag correspond to summer conditions, when the RdlP waters are rapidly exported to the deep ocean (Figure 6a). During this season, the tracer at the shelfbreak is strongly correlated with the tracer over the southern shelf and over the offshore region, and anticorrelated with the tracer along the South American coast. The correlations at the 100 day time lag relate the tracer concentrations at the shelfbreak and along the South American coast (Figure 6b). These patterns correspond with winter conditions, when the tracer is advected along the coast before being detrained into the deep ocean. The 100 day time lag represents the time that it takes the coastal waters to reach the deep ocean. The lack of significant correlations between the shelfbreak and the deep ocean (at this time lag) reflects the fast decorrelation time scales set by the BMC; after reaching the shelfbreak the RdlP waters are rapidly detrained and diluted in the deep ocean waters, so that after a relatively short period the system loses its memory (Figure 6b).

## 6. Salinity and Mixing

### 6.1. Sensitivity to External Forcing

To assess the contributions of the wind stress forcing and the river discharge to the vertical mixing of the plume, we conducted an ancillary suite of sensitivity experiments. The benchmark case is the standard run described in the previous sections. The setup of the other experiments is identical to the benchmark case, except for the following changes: EXP1 is forced with monthly mean winds; EXP2 is forced with climatological monthly mean winds; and EXP3 is forced with daily winds but an average (and constant) RdlP discharge of 24,000 $m^3/s$. The RdlP discharge in EXP1 and EXP2 is the same as in the benchmark case (monthly

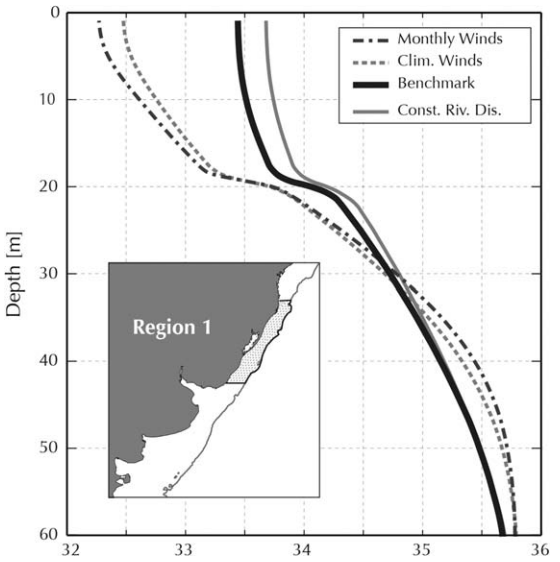


**Figure 7.** Vertical salinity profiles averaged in Region 1 (inset). EXP1: monthly winds; EXP2: climatological winds; EXP3: constant LPR discharge (24,000 $m^3/s$).

values). All the sensitivity experiments are run for the same period as the benchmark experiment (from 2001 to 2012). The changes in vertical mixing associated with the sensitivity experiments are evaluated through the comparison of vertical salinity profiles (Figure 7), which represent the horizontally averaged values of salinity in Region 1 during the year 2010 (Figure 1). We choose the year 2010 for our model intercomparison because it is preceded by the 2009 Niño, which generated an exceptional RdlP discharge of ~53,000 $m^3/s$.

The vertical salinity profiles of all the experiments are characterized by a shallow halocline (~20 m) separating the fresher surface waters from the saltier waters below (Figure 7). The comparison of all the salinity profiles indicates that the high-frequency component of the wind stress forcing is the dominant mixing mechanism of the shelf waters. The differences between EXP1 (monthly wind forcing) and EXP2 (climatological wind forcing) are relatively small. The monthly averaged winds during 2010 had a smaller intensity than the climatology and produced slightly weaker vertical mixing. Other years have a reverse pattern but the differences between EXP1 and EPX2 are always small. There is, however, a substantial difference in stratification between EXP1 and EXP2 and the benchmark case (for the same year), as seen in the steep salinity gradient between the surface and the halocline in EXP1 and EXP2 (~1 PSU per 20 m). The benchmark experiment, however, shows a nearly homogeneous top layer. The difference between these two sets of experiments highlights the importance of high-frequency winds to the vertical mixing of the shelf waters. It should be noted, however, that the high-frequency components of the wind stress forcing do not exert a significant influence on the low-frequency SSS variability. The EOF modes of EXP1, for example, are nearly identical to those of the benchmark case.

EXP3 allows us to evaluate the contribution of above average changes of the RdlP discharge on the salinity structure of the shelf. As noted above, the RdlP has relatively small seasonal variations of its discharge; the largest variations occur at interannual time scales. The comparison of the benchmark case with EXP3, therefore, shows that the largest interannual extremes of discharge create differences of several tenths of a PSU in the upper 20 m and much smaller differences in the next 20 m, but do not noticeably change the stratification.

In summary, the sensitivity study indicates that the high-frequency component of the wind stress forcing controls the mixing properties in the plume waters over the shelf. The lack of change in the EOFs indicates that the low-frequency component of the winds controls the horizontal spreading of the plumes. High-frequency wind variability and interannual variations of the RdlP discharge are the most important contributors to the average salinity of the upper 20 m above the halocline.

### 6.2. The Pathways of Mixing

During their journey through the shelf, the RdlP waters are subject to intense mixing with ambient waters so that by the time these waters reach the deep ocean, their physical and chemical properties have been substantially altered. To evaluate the impact of this mixing on the SSS characteristics, we released neutrally buoyant floats at the mouth of the estuary and tracked their salinity variations as they drift toward the deep ocean. Floats (1612) were released every 10 days starting in 8 January 2008 and ending in 23 December 2008. The float trajectories were calculated offline using a 2 day average of the 3-D velocity field of the model. Each float was tracked for a period of 540 days. Of the 50,156 floats released 38,548 left the shelf within the mixed-layer and 10,608 at depths larger than 50 m.

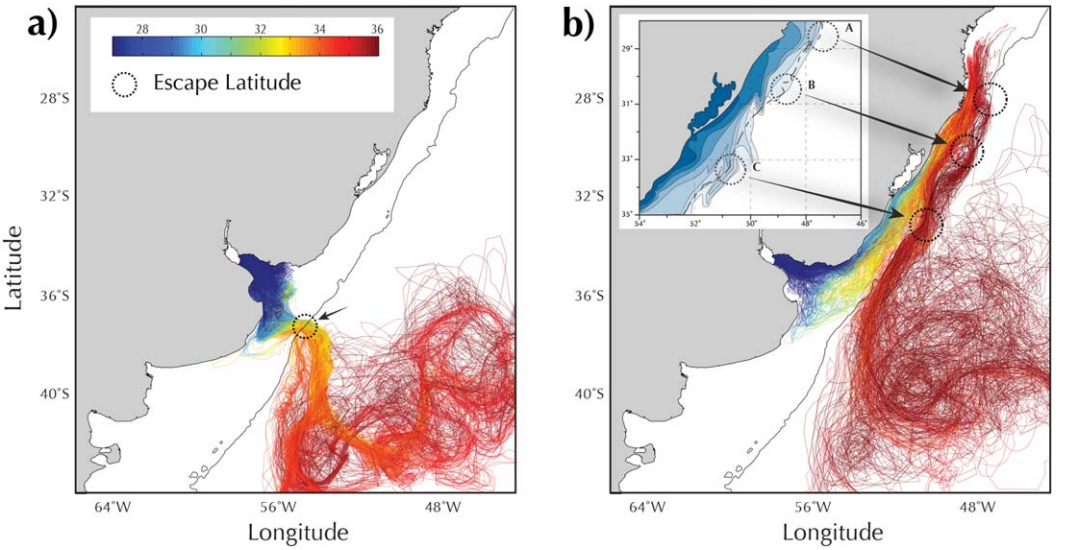


**Figure 8.** Float trajectories. (a) Upstream pathway; (b) downstream pathway. The color corresponds to the salinities along those trajectories. The inset of Figure 8b shows the SSS observed by *Piola et al.* [2008]. The dotted circles mark the location of offshore detrainments. The black contour marks the location of the shelfbreak (200 m isobath).

The float trajectories span the entire latitudinal range from the BMC to Cape Santa Marta (28°S). To illustrate the salinity evolution along the two most extremes cases we chose two subgroups of float trajectories representing the downstream pathway (floats that went past 28°S), and the upstream pathway (floats that crossed the shelfbreak south of 36°S) (Figure 8). The upstream pathway represent summer conditions, when upwelling favorable winds move the floats southward along the coast of Argentina until an opposing flow from the Patagonian shelf displaces them toward the shelfbreak; there the BMC circulation rapidly advects the floats into the deep ocean (Figure 8a). The downstream pathways represent the winter conditions, when the winds reverse direction moving the floats in the downstream direction along the coasts of Uruguay and Brazil, whence they are funneled into the Brazil Current and advected toward the BMC (Figure 8b). Water parcels following the upstream pathway arrive at the shelfbreak with a lower salinity than those following the downstream pathway. The difference is partly attributed to the shortness of the upstream path and partly to the fact that upstream excursions are accompanied by the formation of a bulge of relatively freshwaters, which screens the bulk of the RdlP waters from intense mixing with the ambient waters (Figure 5a). In contrast, the narrow and elongated corridor associated with the downstream spreading favors more mixing with the ambient waters (Figure 5b). In addition, water parcels diverted in the upstream direction mix with relatively fresh Sub-Antarctic Shelf Waters while those diverted downstream are mixed with the much saltier Subtropical Shelf Waters.

To better quantify the impact of mixing, we gathered all the floats trajectories and normalized their travel time by the time that it took each float to reach the shelfbreak. Thus, a normalized time $>1$ corresponds to floats that are in the deep ocean while those with a normalized time $<1$ are over the shelf (regardless of the speed at which the float moved). The superposition of all the trajectories generates a spaghetti diagram that highlights the wide range of SSS variability captured by the floats during their journey toward the deep ocean (Figure 9). The thick lines superimposed on this diagram correspond to the mean SSS variations along the upstream (blue) and the downstream (red) pathways. On average, a float following the downstream path takes approximately 284 days to reach the shelfbreak while a float following the upstream path takes 123 days. These estimates included the approximately 40 days that it takes the floats to travel from their release site in the inner portion of the estuary to the mouth of the RdlP. The salinity signatures of the two pathways start to diverge as soon as the floats leave the estuary (Figure 9b). The downstream pathway shows a steeper salinity increase. It takes, for example, $\sim$0.45 units of normalized time (on average 127 days of real time), to go from 10 to 30 PSU along the downstream pathway and $\sim$0.91 units of normalized time (on average 113 days) along the upstream pathway. The difference, $\sim$2 weeks, is accentuated by the fact that water parcels following the upstream path are very close to the shelfbreak while those following the

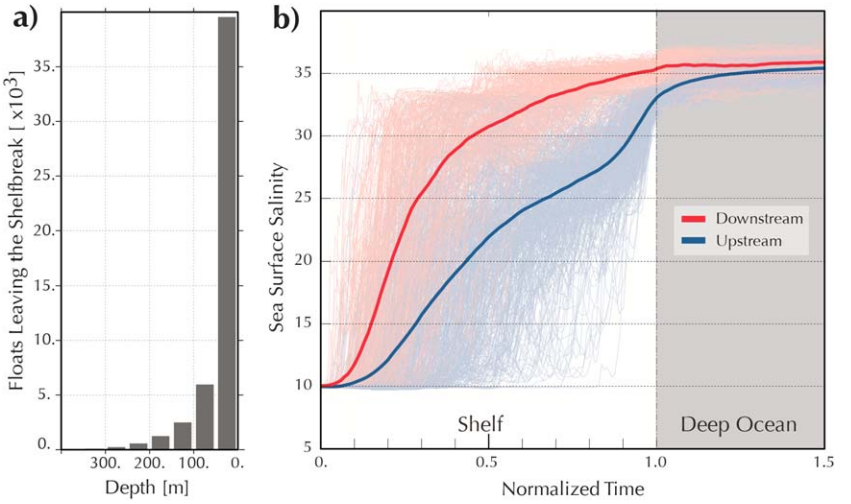


**Figure 9.** Float trajectories in coordinates of salinity and normalized time. (a) Statistics of the final vertical distribution of the floats; (b) spaghetti diagram of all the float trajectories. Red lines correspond to those following the downstream path and the blue lines those following the upstream path. The thick lines are the mean trajectories along the respective paths. Time in Figure 9b is normalized by the time that each float took to reach the shelfbreak. Thus, all the floats with a normalized time smaller than 1 are still over the shelf.

downstream path have not yet reached the middle point of their journey. The upstream pathway shows an abrupt increase of salinities near the shelfbreak (Figure 9b). This increase is produced by an onshore intrusion of the Malvinas Current, which forms a midshelf jet flowing past the BMC [*Palma et al*., 2008; *Matano et al*., 2010]. At the shelfbreak there is an approximate difference of 3 PSU between the two pathways.

One important difference between the upstream and the downstream pathways is that a substantial portion of upstream floats are diverted toward the Southern Ocean while most of the downstream floats are retained in the subtropical gyre (Figure 8). Another important difference is that while the upstream pathway has just one exit point (the BMC, Figure 8a) the downstream pathway has several (Figure 8b). The downstream trajectories, for example, show three locations (marked by the stippled lines and arrows in Figure 8b), where the shelf waters are ejected into the Brazil Current. After leaving the shelf the floats continue along the deep ocean side of the shelfbreak until reaching the BMC where they are expelled into the deep ocean. The existence of multiple exit points along the downstream path is supported by observations. *Piola et al*. [2008a, 2008b], for example, identified four narrow tongues of Sub-Tropical Shelf waters traversing the shelfbreak and intruding into the deep ocean in the region between 35°S and 28°S (Figures 5 and 6a). Snapshots from Aquarius also show similar extrusions of low-salinity waters in the exit points identified by the model (see Figures 5, 9, and supporting information S2 in G14). Animations of the model's velocity field indicate that these extrusions are associated with the interaction between the shelf circulation and the Brazil Current eddies, which, during their poleward travel, intrude onto the shelf and advect the coastal waters into the deep ocean (see Movie_SSS in supporting information). The preferred locations for the offshore detrainments are near protrusions of the shelfbreak, which indicates that the flow over the shelf is influenced by the bottom topography. *Palma and Matano* [2009] have argued that this type of detrainments/entrainments along the shelfbreak is caused by variations of the alongshelf pressure gradient.

## 7. Model and Observations

### 7.1. Seasonal SSS Variability in the Model, In Situ Observations and Aquarius

To assess the realism of the seasonal variations simulated by the model, we compare the summer (DJF) and winter (JJA) SSS fields from the model with in situ and Aquarius observations (Figure 10). The in situ observations include 34,090 bottle and CTD observations collected between 1911 and 2004. Gaps in the historic observations were filled with data from the World Ocean Atlas. To reduce the biases introduced by land contamination, we masked Aquarius data closer than 100 km to the coast. Note that, perforce, the three seasonal estimates cover different periods of time. The model encompasses the period 2001–2012, the in situ observations the period 1911–2004, and the Aquarius data the period September 2011 to September 2013.

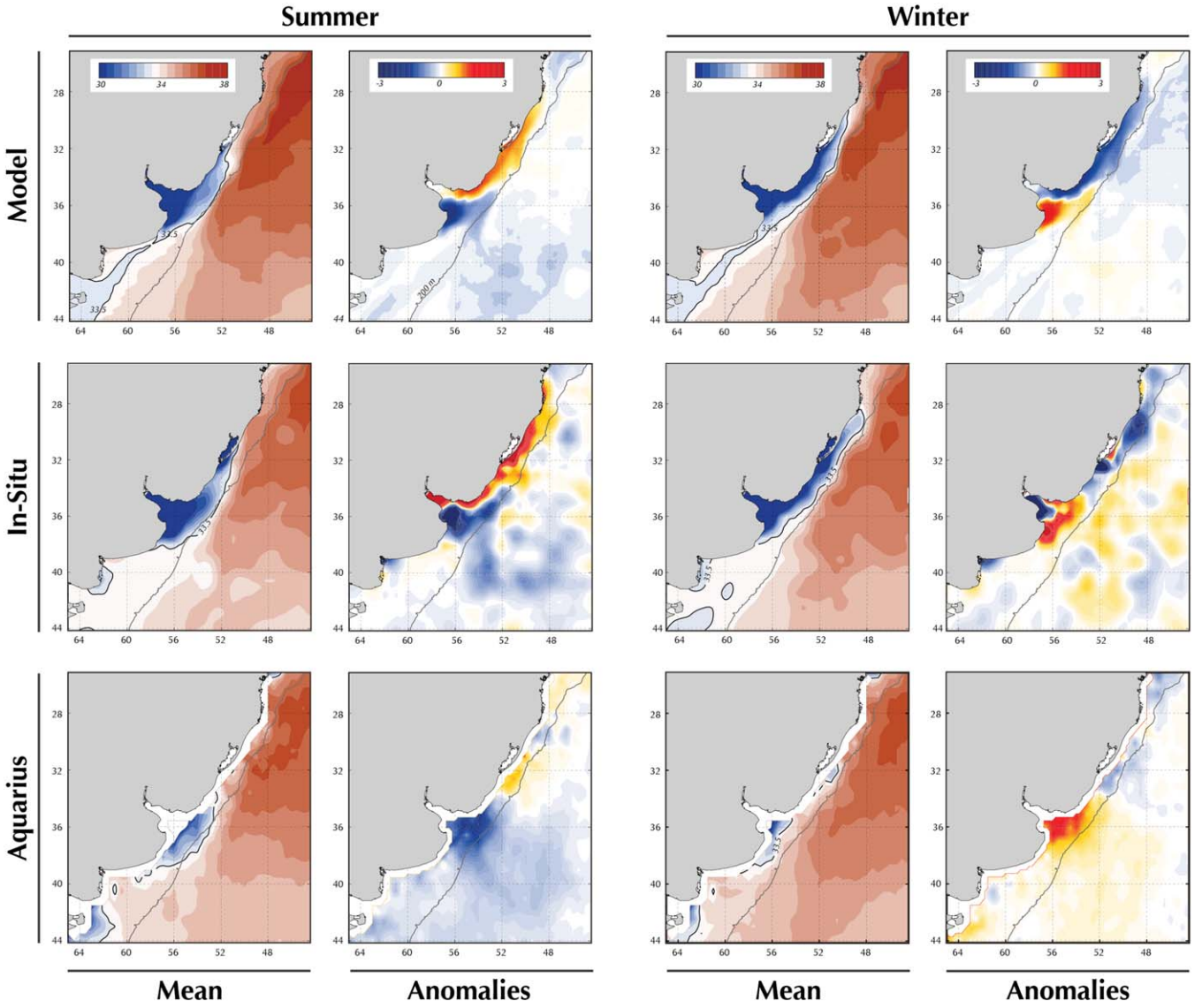


**Figure 10.** (top) Comparison of the seasonal SSS fields in the model, (middle) in situ observations, and (bottom) Aquarius SSS data. The two left plots show the mean values and the two right plots the anomalies (annual average minus the season average).

Model and in situ observations have similar seasonal SSS variations over the shelf (Figure 10). Both data sets show that, during the winter, there is a narrow tongue of freshwater extending northward along the South American coast, while during the summer this tongue retracts southward and expands offshore. The summer retraction of the RdlP waters creates positive SSS seasonal anomalies (annual mean minus the seasonal values) in the northern portion of the shelf—particularly along the boundaries of Uruguay and southern Brazil—and negative SSS anomalies in the southern domain. This situation is reversed during the winter months when, under the influence of downwelling winds, the plume becomes trapped to the coast and extends northward up to approximately 28°S. This northward displacement generates large negative anomalies in the downstream region and positive anomalies in the upstream region. Aquarius cannot detect the nearshore displacement of the low-salinity plume, due to the land mask. Aquarius, however, also shows an offshore expansion of the low-salinity waters during the summer, which is consistent with model and the in situ observations.

The three data sets show similar SSS anomalies in the offshore region. During the summer, for example, the in situ observations show a C-shaped, low-salinity tongue extending from the shelf into the deep ocean south of 34°S. The model reproduces a similar structure, albeit with smaller SSS gradients. The C-shaped

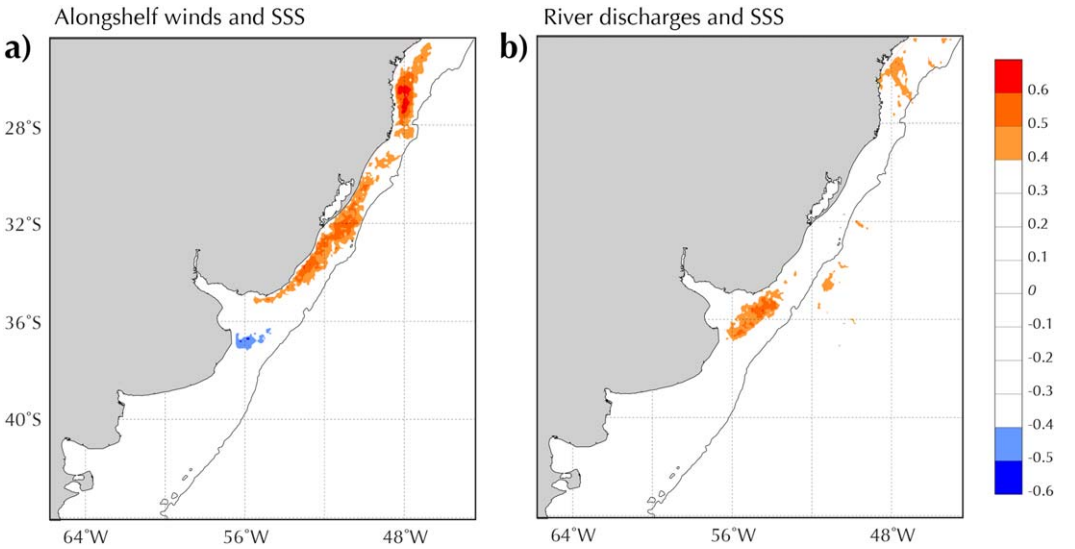


**Figure 11.** Correlation coefficient between an SSS proxy and (a) the alongshelf component of the wind stress forcing and (b) the LPR discharge. The SSS proxy was constructed using satellite estimates of surface chlorophyll-a concentration collected during the period 1998–2005. Adapted from *Piola et al*. [2008].

tongue is not well defined in the Aquarius data, due to the lack of spatial resolution. Aquarius data, however, also show a low-salinity intrusion extending from the continental shelfbreak into the deep ocean. Considering the different origins and the different time spans encompassed by our three sources of information, the similarity of the SSS patterns is quite reasonable. As shown in section 5, the intrusion of the shelf waters into the deep ocean is largely controlled by the dynamics of the western boundary currents. In fact, the C-shaped tongue just described roughly follows the mean location of the BMC.

The model shows two conspicuous differences with the observations. First, it shows biases over the deep ocean and the shelf. Over the deep ocean the model generates saltier waters than observed, while over the Patagonian shelf it generates fresher waters. These biases reflect errors in the freshwater fluxes imposed on the model. In addition, although in situ observations suggest that the SSS in the southern midshelf region is relatively stable, there may still be relatively small variations (∼0.1–0.2) not properly resolved by the observations [see e.g., *Guerrero et al*., 2010]. The inclusion of a restoring term to the salinity equation of the model could have corrected the observed bias but we decided not to use this approach, because the observed biases are relatively small and the use of a correction term to the salinity equation would have hampered the dynamical interpretation of the model results.

The second difference is that the freshwater plume signature extends farther downstream in the observations than in the model. This difference most likely reflects the fact that the model was forced with a constant Patos/Mirim discharge of 2000 $m^3$/s and although historic observations indicate that this might be a reasonable approximation to the average discharge, individual records show peaks of up to 12,000 $m^3$/s [*Möller et al*., 2001]. Having no other reliable information to input into the model, we used the mean value stated above.

### 7.2. EOF Modes of SSS Variability: Model and Observations

The first two EOF modes of our model, which represent the alongshelf displacements of the RdlP and the Patos/Mirim freshwater plumes, are in good agreement with observational results. *Piola et al*. [2008a], for example, found that the highest correlations between the alongshelf winds and a SSS proxy are observed along a relatively narrow corridor hugging the South American coast (Figure 11a) [adapted from *Piola et al*., 2008a, 2008b]. There is a close correspondence between the correlation patterns found by *Piola et al*. [2008a] and the spatial amplitudes of the first EOF of the model (Figure 3). Both estimates, for example, show dipole structures with lobes of opposite signs in the upstream and downstream portions of the continental shelf. *Piola et al*. [2008] also reported that the largest correlations between the alongshelf winds and the SSS proxy have a 2 month time lag. This time lag corresponds well with the 45 days estimated from our

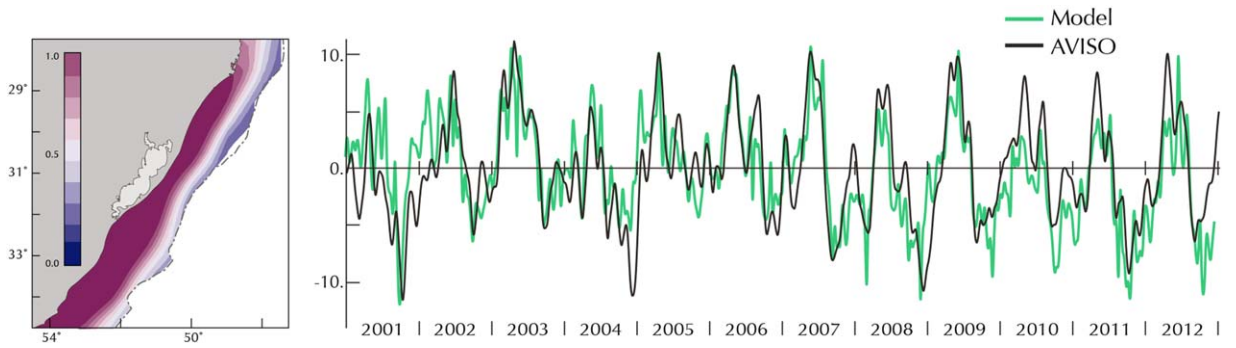


**Figure 12.** Spatial amplitude and time series of the first EOF mode of SSH variability from the AVISO data set. The black line of the time series corresponds to AVISO, the green line to the child model. The spatial amplitude of the first EOF from the model is nearly identical to the AVISO (not shown).

spectral analysis. The 2 week difference between the two estimates is accounted by the fact that *Piola et al*. [2008a] used monthly mean winds while we used daily winds. The second EOF of the model also compares well with the correlation patterns estimated by *Piola et al*. [2008a] (Figure 11b). In agreement with the model results they also found that the largest correlations between the RdlP discharge and the SSS proxy are constrained to the mouth of the river, thus reinforcing the conclusion that the variations of the river discharge do not contribute significantly to the SSS variability away from the source region.

### 7.3. EOF Modes of SSH Variability: Model and Observations

To further assess the model realism, we also compared the SSH variability of the model with gridded altimeter sea level anomaly (SLA) data from the AVISO (Archiving, Validation and Interpretation of Satellite Oceanographic data) research quality (delayed delivery) data set. Although concerns about errors in the tidal models have been especially critical over the Patagonia shelf in the past, the tides over the shelf north of 40°S are much less energetic than farther south [*Palma et al*., 2004b]. In addition, *Saraceno et al*. [2010] have found good agreement between the tidal models used in AVISO corrections and in situ observations north of 42°S on the Patagonia shelf. Land contamination of the altimeter data within ~30 km of the coast is less of a problem for this "coastal" Region 1, since most of the SSH signal over this wide shelf originates far from the coast. In Figure 12, we present the first EOF (explaining 57% of the variance) of AVISO SLA (from the weekly 1/4° weekly gridded data) over the shelf inshore of the 200 m isobath in Region 1 (27.7°S–34.7°S). This region is far north of the region where large tides may cause problems for the altimeter data retrievals. The gradient in the SLA field from the EOF depicts alongshore geostrophic flow over the outer shelf in the south and the midshelf in the north, with a time series (in black) that is typically positive (indicating equatorward flow) from March–August and negative (poleward) from September–February. The spatial pattern of SSH from the model first EOF (explaining 84% of the variance) is not shown because it is nearly identical to that from the altimeter. The time series from the model first EOF (in green) has been interpolated to the weekly AVISO times and both time series have been smoothed with a 5 point boxcar filter. The agreement between the two time series is exceptionally good ($r = 0.79$), given that no data have been assimilated into the model. The agreement of the second EOF time series (not shown, explaining another 8–10% of the variance for both) is moderately good, capturing the lower frequency seasonal changes but missing many intraseasonal peaks and troughs ($r = 0.36$). This level of agreement indicates that the model reproduces a majority of the wind-driven large-scale circulation over the shelf on time scales of 1–2 months and longer, including the seasonal cycle and its variability on intraseasonal and interannual scales. The agreement also serves to validate the use of the altimeter data over the shelf in this region and on these scales, as reported by *Saraceno et al*. [2010], *Strub et al*. [2014], and (Strub et al., 2014, in preparation).

## 8. Summary and Final Remarks

We identify three dominant modes of SSS variability. The first two, which have been discussed in previous studies, represent the seasonal variations of the RdlP and the Patos/Mirim plumes over the continental shelf. The third mode of SSS variability, which has not been discussed hitherto, represents the salinity exchanges between the shelf and the deep ocean. The seasonal oscillations of this mode are partly driven by the

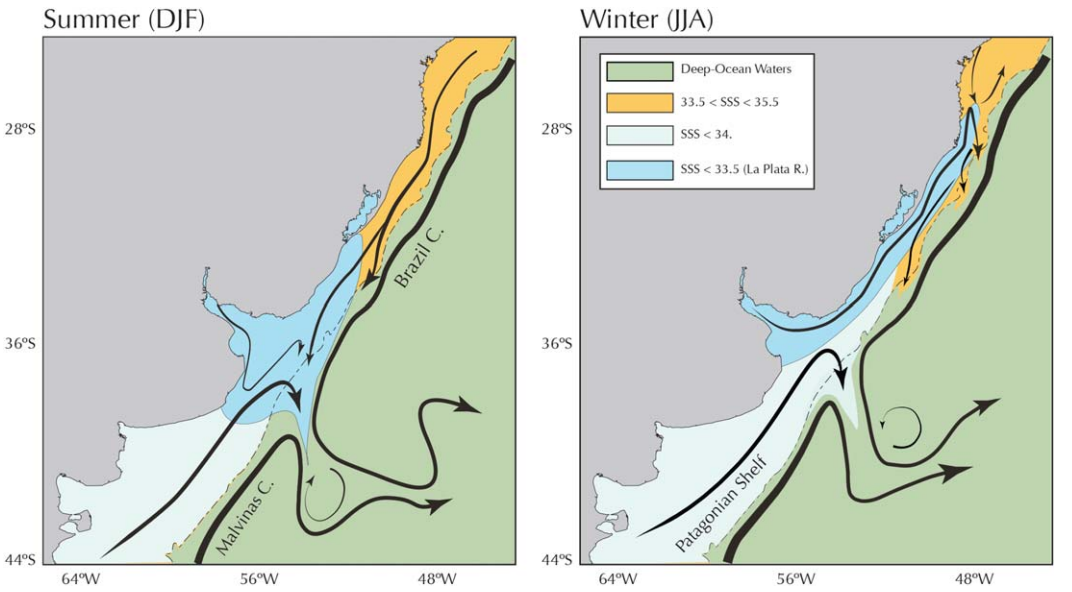


**Figure 13.** Schematic of the SSS and circulation in the southwestern Atlantic region during summer and winter. The regions filled with light blue represent the spreading of the LPR and Patos/Mirim freshwater plumes. This schematic is based on the annual mean patterns from the child model and in situ observations.

dynamics of the western boundary currents and partly by the local wind stress forcing. A diagnostic study using floats and passive tracers identifies the pathways taken by the freshwater plumes. During the winter, northeasterly winds generate geostrophic currents that advect the plumes downstream leaving the shelf region north of the BMC (Figure 13). The low-salinity waters reaching the BMC during this season are drawn from the Patagonian shelf. During the summer, southwesterly winds generate currents that arrest the downstream spreading of the plumes funneling them into the BMC (Figure 13). Float trajectories suggest that the final destination of the shelf waters depends on their pathway over the shelf. The upstream pathway (summer) favors entrainment into the Southern Ocean. The downstream pathway (winter) favors entrainment into the Subtropical Gyre.

To further investigate the connection between SSS anomalies and cross-shelf exchanges, we computed a volume balance of the shelf region between 34°S and 38°S (Figure 14). The annual mean off-shelf transport in this region is 1.21 Sv. Most of this transport is drawn from the Patagonian Shelf (1.15 Sv); the contributions from the RdlP discharge (0.024 Sv) and the Brazilian shelf (0.038 Sv) are quantitatively insignificant.

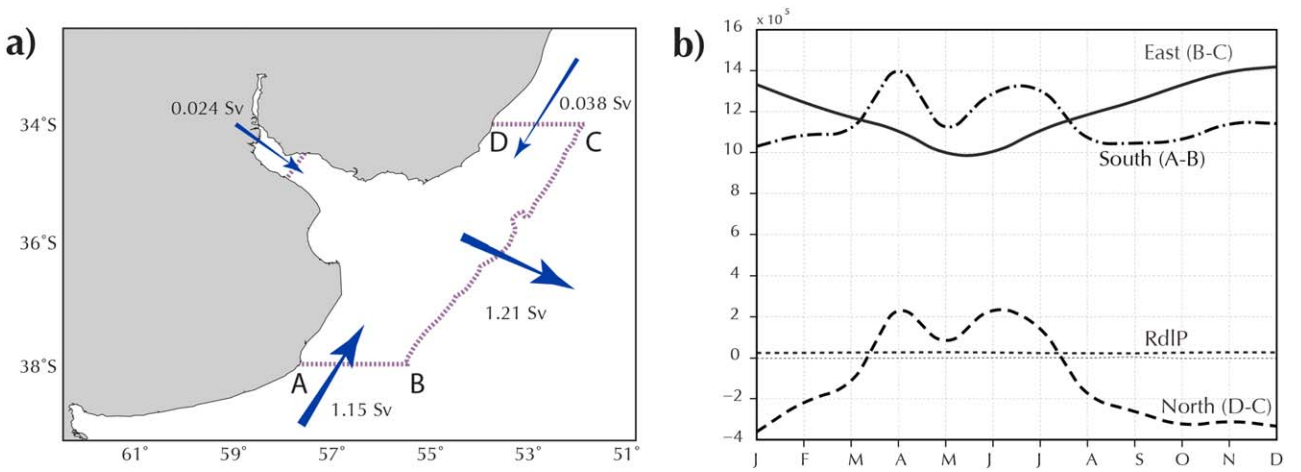


**Figure 14.** Volume balance. (a) The dotted line marks the shelf region where the balance was made. It extends from 34°S to 38°S and from the coast to the 200 m isobath; (b) seasonal evolution of the volume fluxes in the four open boundaries.

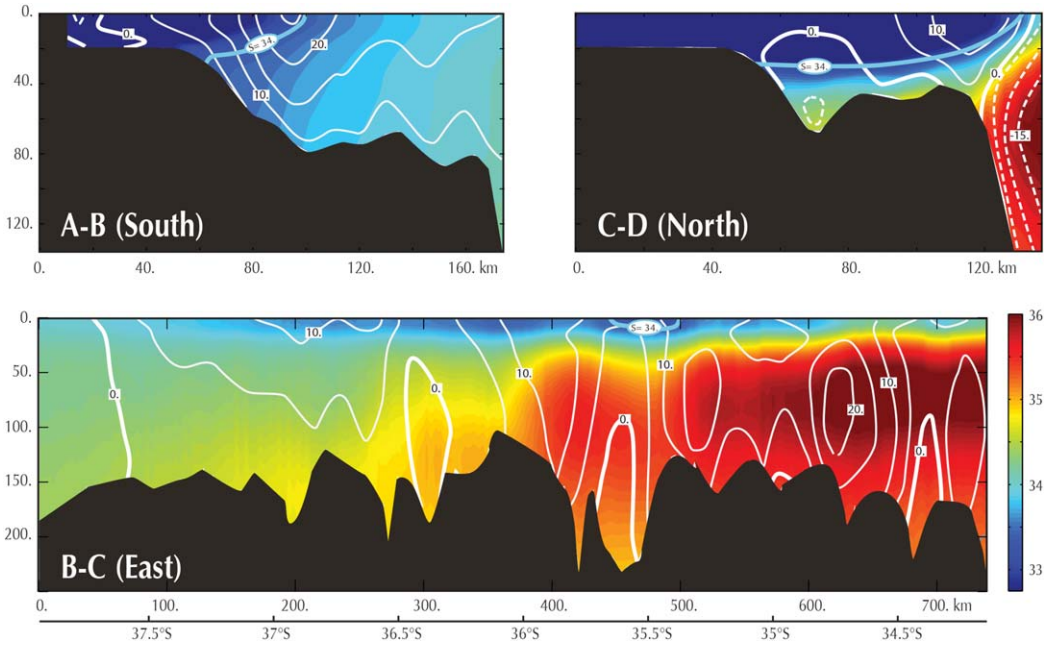


**Figure 15.** Mean vertical structure of the cross sections shown in Figure 14. The background colors represent the salinity field and the white contours are for the velocities (cm/s). The light-blue contours mark the 34 isohaline, which represents the limit of the LPR waters.

The seasonal variations of the off-shelf transport are relatively small and out of phase with the variations of the Patagonian mass flux; it decreases during the winter and increases during the summer. During the winter, a substantial portion of the Patagonian waters and the RdlP waters are funneled toward the Brazilian shelf, thus reducing the net off-shelf flux.

Vertical profiles across the box boundaries illustrate the relation between volume and salinity fluxes (Figure 15). The southern cross section (A–B) is characterized by the presence of low-salinity waters against the coast, which are associated with the upstream (southward) extension of the RdlP plume. The plume is vertically homogeneous in the inner shelf, detaches from the bottom at ∼25 m depth and extends offshore as a surface-trapped plume. The corresponding velocity field shows an upstream jet near the coast that advects the RdlP plume waters south and a stronger midshelf jet flowing in the opposing direction. The northern cross section (C–D) shows a deep, midshelf channel filled with saltier Subtropical Shelf Waters flowing poleward underneath the fresher waters from the RdlP plume. Farther offshore, this cross section shows a northward flowing jet, which is an onshore intrusion of the Malvinas Current [*Palma et al*., 2008; *Combes and Matano*, 2014]. Past the shelfbreak there is the poleward flow of the Brazil Current, which carries saltier waters toward the BMC. The eastern cross section (B–C) shows a dominant off-shelf flow of 10–20 cm/s in the north (34.5°S–35.5°S) and 5–10 cm/s in the south (35.5°S–37.5°S). The corresponding salinity field shows a shallow layer ($h < 20$ m) of freshwaters capping the saltier waters of the Brazil Current. The seasonal anomalies of the off-shelf flow are relatively small (e.g., Figure 14). During the winter there is a decrease of the off-shelf velocities south of 35°S (∼1–2 cm/s) and an increase farther north (<1 cm/s). These patterns reverse during the summer but the flow always maintains its barotropic structure, which indicates that SSS anomalies represent motions of the entire water column.

Our study region is characterized by a persistent off-shelf mass flux. The contributions of the RdlP and the Patos/Mirim discharges to this flux are quantitatively insignificant but the SSS anomalies associated with them are qualitatively important, not only because they represent net mass exchanges between the shelf and the deep ocean but also because they allow to differentiate the type of surface waters detrained at the BMC: Subtropical Shelf Waters during the winter and Sub-Antarctic Shelf during the summer. Previous studies have shown that seasonal and interannual changes of the water masses participating in these exchanges have a profound impact on the local marine ecosystems [*Auad and Martos*, 2012]. The SSS anomalies generated by the RdlP and the Patos/Mirim discharges also allow the identification of the preferential sites for cross-shelf exchanges. In fact, it has been only through the analysis of Aquarius SSS data that we have been

able to identify these sites (e.g., Figure 9 in G14). Most importantly, the RdlP and Patos/Mirim discharges are important sources for the injection of terrigenous and anthropogenic materials of continental origin into the deep portion of the South Atlantic Ocean, and hence for the basin's carbon cycle. The preliminary analysis presented herein indicates that SSS data could eventually be used to assess what portion of this discharge ends up in the Southern Ocean, in comparison to the subtropical gyre. As a High-Nutrient Low-Chlorophyll region, the Southern Ocean is more easily stimulated to high productivity by the injection of terrigenous iron and other micronutrients, whereas the nutrients added to the oligotrophic subtropical gyre will have less of an impact on productivity. Thus, an assessment of the eventual destination of the entrained water from the SW Atlantic shelf is more important than its small volume flux would imply.

Although the present generation of the salinity remote sensors does not have the resolution needed to make such assessments, future sensors will hopefully have better spatial resolution and sensitivity. However, the restriction of the remotely sensed SSS (and other remotely sensed parameters) to the upper ocean will remain, requiring their combination with in situ data and realistic model simulations. We suggest that the question posed above, i.e., the fate of the shelf water in the SW Atlantic, is a question suitable for future focused studies combining satellite observations, model studies and intensive field sampling of the coastal waters and their ecosystems, following them as they move from the shelf to the deep ocean.

**Acknowledgments**

We dedicate this article to the memory of Hermes W. Mianzan, a good friend and a colleague whose insight and interest in the impact of cross-shelf exchanges on the ecology of the continental shelf was a major motivation for our study. He will be greatly missed. We acknowledge the valuable comments and suggestions of two anonymous reviewers. The SSS data used in this project can be obtained from http://podaac.jpl.nasa.gov/aquarius. R. Matano and V. Combes acknowledge the financial support of NASA through grants NNX08AR40G and NNX12AF67G, NOAA through grant NA13OAR4310132 and the National Science Foundation through grant OCE-0928348. A. R. Piola, E. D. Palma, M. S., R. A. Guerrero, and H. Fenco acknowledge the financial support of grants 001 and 008 from Comisión Nacional de Actividades Espaciales/Ministerio de Ciencia, Tecnología e Innovación Productiva, Argentina. A. R. Piola and MS also acknowledge the support of grants SGP2076 and from the Inter-American Institute for Global Change Research, through the US National Science Foundation grants GEO-0452325 and GEO-1128040. E. D. Palma, A.RP and MS also acknowledge the support from Agencia Nacional de Promocion Cientifica y Tecnologica Grant PICT08–1874. P. T. Strub and C. James acknowledges the financial support of NASA through grants NNX08AR40G and NNX10A092G. Y.C. is funded by the NASA Ocean Salinity Science Team grant at UCLA through a subcontract to grant NNX08AR40G. M. Saraceno also acknowledges support from EUMETSAT/CNES DSP/OT/12-2118 and CONICET-YPF PIO 133-20130100242.

## References

Auad, G., and P. Martos (2012), Climate variability of the northern Argentinean shelf circulation: Impact on *Engraulis Anchoita*, *Int. J. Ocean Clim. Syst.*, *3*, 17–43.

Combes, V., and R. P. Matano (2014), A two-way nested simulation of the oceanic circulation in the Southwestern Atlantic, *J. Geophys. Res. Oceans*, *119*, 731–756, doi:10.1002/2013JC009498.

Clarke, R. T. (2005), The relation between interannual storage and frequency of droughts, with particular reference to the Pantanal Wetland of South America, *Geophys. Res. Lett.*, *32*, L05402, doi:10.1029/2004GL021742.

Depetris, P. J., S. Kempe, M. Latif, and W. G. Mook (1996), ENSO controlled flooding in the Paraná River (1904–1991), *Naturwissenschaften*, *83*, 127–129.

Framiñan, M., M. Etala, M. Acha, R. Guerrero, C. Lasta, and O. Brown (1999), Physical characteristics and processes of Rio de La Plata estuary, in *Estuaries of South America*, edited by G. Perillo, M. Piccolo, and M. Pino-Quivira, pp. 161–194, Springer, N. Y.

Goni, G. J., and I. Wainer (2001), Investigation of the Brazil Current front variability from altimeter data, *J. Geophys. Res.*, *106*, 31,117–31,128,.

Gordon, A. L. (1989), Brazil–Malvinas confluence—198, *Deep Sea Res., Part A*, *36*, 359–384, doi:10.1029/2000JC000396.

Guerrero, R., E. Acha, M. Framinan, and C. Lasta (1997), Physical oceanography of Rio de La Plata estuary, Argentina, *Cont. Shelf Res.*, *17*, 727–742.

Guerrero, R. A., A. R. Piola, H. Fenco, R. P. Matano, V. Combes, Y. Chao, C. James, E. D. Palma, M. Saraceno, P. T. Strub (2014), The salinity signature of the cross-shelf exchanges in the southwestern Atlantic Ocean: Satellite observations., *J. Geophys. Res. Oceans*, *119*, doi:10.1002/2014JC010113.

Guerrero, R. A., A. R. Piola, G. N. Molinari, A. P. Osiroff, and S. I. Jauregui (2010), *Climatología de temperature y salinidad en el Rio de la Plata y su frente marítimo*, 95 pp., Argentina y Uruguay, Inst. Nac. de Invest. y Desarrollo Pesquero, Mar del Plata, Argentina.

Liu, Y., X. S. Liang, and R. H. Weisberg (2007), Rectification of the bias in the wavelet power spectrum, *J. Atmos. Oceanic Technol.*, *24*(12), 2093–2102.

Matano, R. P., and E. D. Palma (2010a), The upstream spreading of bottom-trapped plumes, *J. Phys. Oceanogr.*, *40*, 1631–1650, doi:10.1175/2010JPO4351.

Matano, R. P., and E. D. Palma (2010b), The spin-down of bottom-trapped plumes, *J. Phys. Oceanogr.*, *40*, 1651–1658, doi:10.1175/2010JPO4352.1.

Matano, R. P., and E. D. Palma (2013), The impact of boundary conditions on the upstream spreading of bottom-trapped plumes, *J. Phys. Oceanogr.*, *43*, 1060–1069, doi:10.1175/JPO-D-12-0116.

Matano, R. P., M. G. Schlax, and D. B. Chelton (1993), Seasonal variability in the southwestern Atlantic, *J. Geophys. Res.*, *98*, 18,027–18,035.

Matano, R. P., E. D. Palma, and A. R. Piola (2010), The influence of the Brazil and Malvinas Currents on the Southwestern Atlantic Shelf circulation, *Ocean Sci.*, *6*, 983–995.

Möller, O. O., Jr., P. Castaing, J.-C. Salomon, and P. Lazure (2001), The influence of local and non-local forcing effects on the subtidal circulation of Patos Lagoon, *Estuaries*, *24*, 297–311.

Möller, O. O., Jr., A. R. Piola, A. C. Freitas, and E. J. D. Campos (2008), The effects of river discharge and seasonal winds on the shelf off Southeastern South America, *Cont. Shelf Res.*, *28*, 1607–1624.

Olson, D., G. P. Podesta, R. H. Evans, and O. B. Brown (1988), Temporal variations in the separation of Brazil and Malvinas currents, *Deep Sea Res., Part A*, *35*, 1971–1990.

Palma, E. D., and R. P. Matano (2009), Disentangling the upwelling mechanisms of the South Brazil Bight, *Cont. Shelf Res.*, *29*, 1525–1534, doi:10.1016/j.csr.2009.04.002.

Palma, E. D., R. P. Matano, and A. R. Piola (2004a), A comparison of the circulation patterns over the southwestern Atlantic shelf driven by different wind climatologies, *Geophys. Res. Lett.*, *31*, L24303, doi:10.1029/2004GL021068.

Palma, E. D., R. P. Matano, and A. R. Piola (2004b), A numerical study of the Southwestern Atlantic Shelf circulation: Barotropic response to tidal and wind forcing, *J. Geophys. Res.*, *109*, C08014, doi:10.1029/2004JC002315.

Palma, E. D., R. P. Matano, and A. R. Piola (2008), A numerical study of the Southwestern Atlantic Shelf circulation: Stratified ocean response to local and offshore forcing, *J. Geophys. Res.*, *113*, C11010, doi:10.1029/2007JC004720.

Piola, A., E. Campos, O. Moller, M. Claro, and C. Matinez (2000), Subtropical Shelf Front off eastern South America, *J. Geophys. Res.*, *105*, 6565–6578.

Piola, A. R., R. P. Matano, E. D. Palma, O. O. Moller, and E. J. D. Campos (2005), The influence of the Plata River discharge on the western South Atlantic shelf, *Geophys. Res. Lett.*, *32*, L01603, doi:10.1029/2004GL021638.

Piola, A. R., S. I. Romero, and U. Zajaczkovski (2008a), Space-time variability of the Plata plume inferred from ocean color, *Cont. Shelf Res.*, *28*, 1556–1567.

Piola, A. R., O. O. Moller, R. A. Guerrero, and E. J. D. Campos (2008b), Variability of the subtropical shelf front off eastern South America: Winter 2003 and summer 2004, *Cont. Shelf Res.*, *28*, 1639–1648.

Preisendorfer, R. W. (1988), *Principal Component Analysis in Meteorology and Oceanography*, vol. 17, edited by C. D. Mobley, pp. 241–245, Elsevier, Amsterdam.

Provost, C., V. Garcon, and I. Medina Falcon (1996), Hydrographic conditions in the surface layers over the slope-open ocean transition area near the Brazil-Malvinas confluence during austral summer 1990, *Cont. Shelf Res.*, *16*(2), 215–219.

Saraceno, M., E. E. D'Onofrio, M. E. Fiore, and W. H. Grismeyer (2010), Tide model comparison over the Southwestern Atlantic Shelf, *Cont. Shelf Res.*, *30*, 1865–1875.

Shchepetkin, A., and J. C. McWilliams (2005), The regional oceanic modeling system (ROMS): A split explicit, free-surface, topography-following-coordinate oceanic model, *Ocean Modell.*, *9*, 347–404.

Simionato, C. G., M. N. Nuñez, and M. Engel (2001), The salinity front of the Rio de la Plata—A numerical case study for winter and summer conditions, *Geophys. Res. Lett.*, *28*, 2641–2644.

Soares, I. D., V. Kourafalou, and T. N. Lee (2007a), Circulation on the western South Atlantic continental shelf. 1: Numerical process studies on buoyancy, *J. Geophys. Res.*, *112*, C04002, doi:10.1029/2006JC003618.

Soares, I. D., V. Kourafalou, and T. N. Lee (2007b), Circulation on the western South Atlantic continental shelf. 2: Spring and autumn realistic simulations, *J. Geophys. Res.*, *112*, C04003, doi:10.1029/2006JC003620.

Torrence, C., and G. P. Compo (1998), A practical guide to wavelet analysis, *Bull. Am. Meteorol. Soc.*, *79*, 61.